ARTICLE

Single-Crystalline MFe_2O_4 Nanotubes/Nanorings Synthesized by Thermal Transformation Process for Biological Applications

Hai-Ming Fan,[†,‡,*] Jia-Bao Yi,[‡] Yi Yang,[§] Kiang-Wei Kho,[⊥] Hui-Ru Tan,[¶] Ze-Xiang Shen,[#] Jun Ding,[‡] Xiao-Wei Sun,[§] Malini Carolene Olivo,[⊥,∇,○] and Yuan-Ping Feng[†,*]

[†]Department of Physics, National University of Singapore, 2 Science Drive 3, 117542 Singapore, [‡]Department of Materials Science and Engineering, National University of Singapore, 119260 Singapore, [§]School of Electrical and Electronic Engineering, Nanyang Technological University, Nanyang Avenue, 639798 Singapore, [⊥]Division of Medical Sciences, National Cancer Centre, 11 Hospital Drive, 169610 Singapore, [¶]Institute of Materials Research and Engineering, 3 Research Link, 117602 Singapore, [#]Division of Physics and Applied Physics, School of Physical and Mathematical Sciences, Nanyang Technological University, 637616 Singapore, [∇]Department of Pharmacy, National University of Singapore, Science Drive 4, 117542 Singapore, and [○]Singapore Bioimaging Consortium, Biomedical Sciences Institutes, 11 Biopolis Way, 02-02 Helios, 138667 Singapore

ABSTRACT We report a general thermal transformation approach to synthesize single-crystalline magnetic transition metal oxides nanotubes/nanorings including magnetite Fe_3O_4, maghematite γ-Fe_2O_3, and ferrites MFe_2O_4 (M = Co, Mn, Ni, Cu) using hematite α-Fe_2O_3 nanotubes/nanorings template. While the straightforward reduction or reduction-oxides process was employed to produce Fe_3O_4 and γ-Fe_2O_3, the α-Fe_2O_3/$M(OH)_2$ core/shell nanostructure was used as precursor to prepare MFe_2O_4 nanotubes *via* MFe_2O_{4-x} ($0 < x < 1$) intermediate. The transformed ferrites nanocrystals retain the hollow structure and single-crystalline nature of the original templates. However, the crystallographic orientation-relationships of cubic spinel ferrites and trigonal hematite show strong correlation with their morpologies. The hollow-structured MFe_2O_4 nanocrystals with tunable size, shape, and composition have exhibited unique magnetic properties. Moreover, they have been demonstrated as a highly effective peroxidase mimic catalysts for laboratory immunoassays or as a universal nanocapsules hybridized with luminescent QDs for magnetic separation and optical probe of lung cancer cells, suggesting that these biocompatible magnetic nanotubes/nanorings have great potential in biomedicine and biomagnetic applications.

KEYWORDS: nanotubes/nanorings · thermal transformation · cubic spinel ferrites · magnetic properties · biological applications

*Address correspondence to msefhm@nus.edu.sg (H.M.F.), phyfyp@nus.edu.sg (Y.P.F.).

Received for review June 26, 2009 and accepted August 24, 2009.

Published online August 27, 2009. 10.1021/nn9006797 CCC: $40.75

The development of magnetic nanocrystals has been intensively pursued for both fundamental scientific interest and technological applications.[1,2] Among the various magnetic materials, the cubic spinel structured MFe_2O_4 represents an important class of magnetic transition metal oxide materials in which oxygen atoms form an fcc close-packed structure, M^{2+} and Fe^{3+} occupy either the tetrahedral or the octahedral interstitial sites.[3−5] The magnetic properties of these spinel MFe_2O_4 can be effectively engineered by choosing different elements as divalent metal ion (M^{2+}). Nanometer-sized MFe_2O_4 materials and their dispersions have been widely used in many important technological applications ranging from information storage,[6] electronics,[7,8] catalysis,[9] magnetic resonance image (MRI), to biomedicine and drug delivery.[10−12] In particular, they have been considered to be the most promising magnetic materials in biological applications. For example, magnetite (Fe_3O_4) has been used as a tag for sensing and imaging, an efficient peroxidase-like catalyst for immunoassay test and an activity agent for antitumor therapy;[13−15] while $NiFe_2O_4$ nanocrystal has shown its advantage in hyperthermia application.[16] With excellent transparent properties, γ-Fe_2O_3 is an ideal candidate for fabrication of luminescent and magnetic dual functional nano-composites.[17,18]

To achieve high performance in function-specific biological applications, magnetic particles are required to have high thermal and chemical stabilities, large surface areas for maximal protein or enzyme binding, high saturation magnetization to provide maximum signal, and good dispersion in liquid media.[10−15,18,19] Recently, a special class of hollow-structured nanocrystals, nanotubes, and nanorings have attracted considerable attention.[20−22] Compared to solid nanocrystals, these hollow structures have larger surface areas and their hollow interior structure allows external agents to be encapsulated inside. More-

over, the single-crystalline magnetic nanotubes/nanorings may possess vortex domain structure in which the magnetization forms a closure structure without magnetic poles or stray fields. This leads to weak magnetic interparticle interactions that can be utilized to facilitate well-dispersed ferrofluid. Furthermore, the dispersion consisting of vortex nanorings (or curl-domain-structured nanotubes) can provide fast and strong response under relatively small external field to meet increasing demands of various biological applications. All these features of single-crystalline MFe_2O_4 nanotubes and nanorings open up new possibilities for improving existing biological applications and creating new technologies through designing novel materials.[23]

However, the synthesis of single-crystalline magnetic spinel ferrites nanotubes (NTs) and nanorings (NRs) has been a challenge so far. Even though many synthetic arts have been developed in the past 10 years, including rolling up layered precursors,[24,25] physical or chemical etching the core of a single or core−shell nanowire,[26,27] coating pores in templates,[28] and transforming nanowires by Kirkendall effect,[29] synthesizing such hollow nanostructures with controlled size and shape remains difficult. Recently, synthesis of α-Fe_2O_3 NTs and NRs by a simple hydrothermal route based on a dissolution mechanism was reported.[30,31] By varying the concentrations of reactants in hydrothermal process, we have also successfully demonstrated the shape-controllable synthesis of α-Fe_2O_3 hollow nanocrystals.[32] Nevertheless, attempt to synthsize MFe_2O_4 NTs/NRs by the same solution-phase route was not successful because the formation of MFe_2O_4 NTs/NRs requires relatively high pH value and the dissolution process is prohibited under such condition.[5]

Thermal transformation of phase and structure from one inorganic material to another *via* gas−solid or solid−solid reaction is a common approach for fabrication of novel functional materials.[33] Compared to bulk materials, nanocrystals have less volume defect and better flexibility (enhanced yielding strength) which make it easier for them to undergo a phase transformation by oxidation/reduction process, or for another element to be introduced without changing the structural and single-crystalline properties.[34] In the present work, we demonstrate that by elaborate control of the gas−solid and solid−solid reaction conditions in the thermal transformation process, single-crystalline trigonal Fe_2O_3 NTs/NRs can be rationally transformed into cubic spinel magnetite Fe_3O_4, maghemite γ-Fe_2O_3, or ferrite MFe_2O_4 (M = Co, Mn, Ni, Cu) without affecting their morphology and single-crystalline nature. The overall synthetic procedure is schematically shown in Scheme 1. Transmission electron miscroscopy, X-ray diffraction, and Raman spectroscopy were employed to understand the thermal transformation mechanism. The magnetic characterizations of the NTs/NRs have been performed to show their dependences on size, shape, and composition. Moreover, we have also explored the potential bioapplications of these magnetic NTs and NRs in catalysis and magnetic separation of cancer cell.

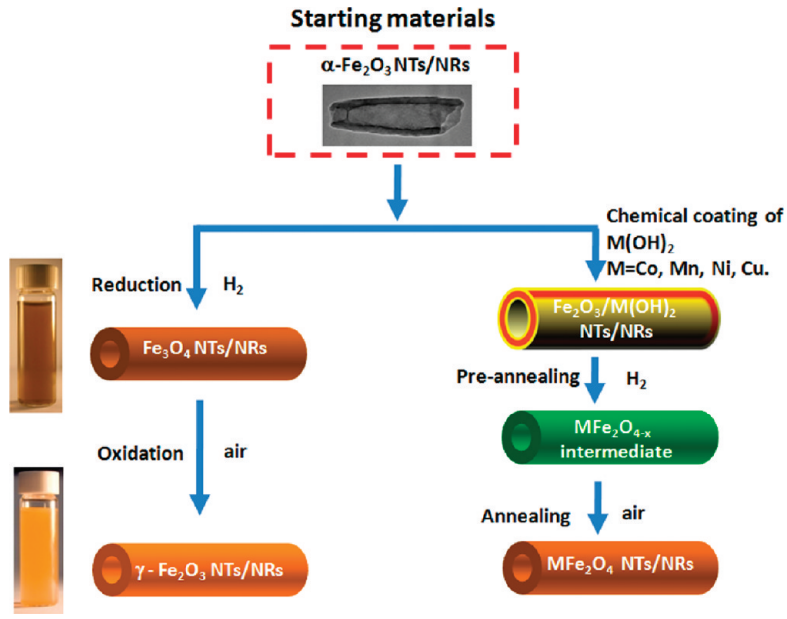

Scheme 1. The Overall Scheme for the synthesis of spinel MFe_2O_4 Nanotubes/Nanorings. The Insets are the Optical Images of Fe_3O_4 and γ-Fe_2O_3 Nanotubes Water Dispersion after Surface Modification by Citric Acid.

RESULTS AND DISCUSSION

Magnetite Fe_3O_4 and γ-Fe_2O_3 Nanotubes. Magnetite Fe_3O_4 nanotubes/nanorings were prepared by direct thermal reduction of α-Fe_2O_3 templates. Temperature programmed reduction (TPR) experiments for different-sized hollow nanocrystals reveal that the transformation temperature decreases with the decreasing size due to finite size effect (Figure S1 in the Supporting Information). Figure 1 shows the TEM images of α-Fe_2O_3 nanotubes template and the Fe_3O_4 product, respectively. As can be seen in parts a and c of Figure 1, the tubular morphology of Fe_3O_4 is perfectly retained during the gas−solid reaction. The high resolution TEM (HR-TEM) images and diffraction patterns shown in parts b and d of Figure 1 clearly indicate that the nanotubes are single-crystalline trigonal α-Fe_2O_3 and cubic spinel Fe_3O_4, respectively, which is also confirmed by XRD results (Figure 5). The tube axes of the α-Fe_2O_3 and Fe_3O_4 nanotubes are in the ⟨001⟩ and ⟨111⟩ direction, respectively. The spacings between lattice planes are 2.7 and 4.8 Å, respectively, which correspond to those of Fe_2O_3 {014} and Fe_3O_4 {111} planes. The crystallographic orientation relationship (OR) of [001]-oriented hematite nanotube and [111]-oriented magnetite nanotube indicates a topotactic transformation.[35] Further oxidation

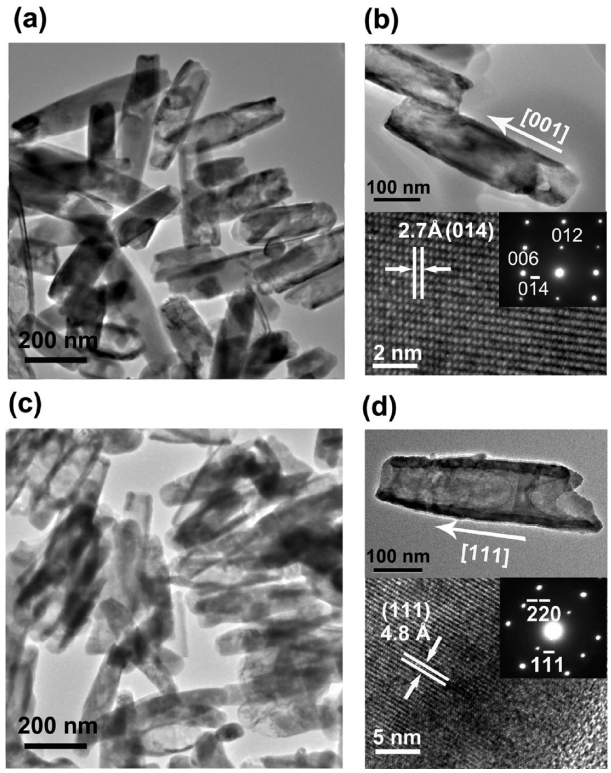

Figure 1. (a) TEM and (b) HRTEM images of α-Fe_2O_3 nanotubes; (c) TEM and (d) HRTEM images of Fe_3O_4 nanotubes. The SAED patterns inserted in panels b and d reveal that (001)-oriented α-Fe_2O_3 nanotubes transformed into single-crystalline (111)-oriented Fe_3O_4 nanotubes.

of magnetite nanotubes in air results in cation-deficient spinel γ-Fe_2O_3 nanotubes, while the single-crystalline nature and tubular morphology are still retained.

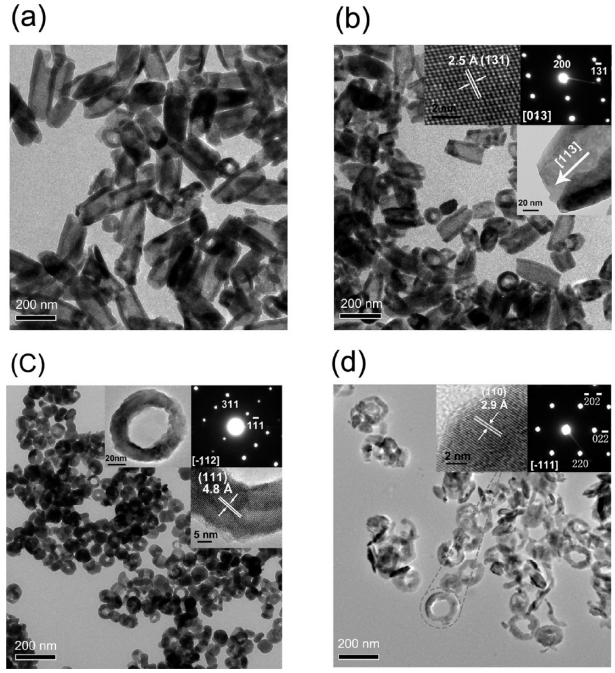

Figure 2. TEM images of transformed Fe_3O_4 hollow structures with various size and crystallographic orientation.

Physical and chemical properties of nanocrystals are strongly dependent on their sizes and shape. Therefore controlling the size and shape of nanocrystals is crucial for technological applications of nanocrystals. By tailoring the size of the α-Fe_2O_3 template, magnetic oxides with various sizes can be produced *via* the phase transformation process. Figure 2 shows the TEM images of magnetite hollow nanocrystals with different sizes and shapes obtained in the present study. Here the average length of the magnetite nanotubes is tuned from 370 nm down to 10 nm. When the aspect ratio becomes small (<1), the nanotubes are transformed into nanorings. The wall thicknesses of these nanotubes and nanorings range from 15 to 40 nm. (Figure S2 and Table S1 in the Supporting Information). TEM analyses indicate that all the magnetite hollow structures are single crystal, and the crystallographic orientation shows a strong correlation with their size. While [111] axis orientation is common in Fe_3O_4 hollow nanocrystals of all sizes, more than 40% of the long tubes (length $>$ 100 nm) were found to have axis along the [113] direction (Figure 2b), and some nanorings with height of 50 nm ($\sim$20%) prefer the [112] direction (Figure 2c). All thin nanorings with height of 10 nm were found to be [111]-oriented. (Figure 2d) (Figure S3 in Supporting Information) Since all trigonal Fe_2O_3 templates have the same [001] crystallographic orientations,[30−32] the appearance of magnetite nanotube with high index [113] and [112] axes implies that the size and morphology of the initial α-Fe_2O_3 templates have significant influence on the crystallographic orientation of final product during the thermal transformation process. Besides the topotactic transformation from [001]-oriented hematite nanotube to [111]-oriented magnetite nanotube, the orientation-relationships of [001] hematite $\rightarrow$ [113] magnetite and [001] hematite $\rightarrow$ [112] magnetite have also been proposed by Becker *et al.*[35] and are attributed to formation of twining dislocation.[36] The change in crystallographic orientation of nanotubes may be due to the minimization of surface energy which is a dominant factor in determining thermodynamics stability of a nanocrystal.[37] For example, the surface free energies of different facets are in the order of $\{111\} < \{100\} < \{110\}$ for the fcc structure,[38] and therefore, the magnetite nanorings in part d of Figure 2 are dominated by [111] axis orientation as the predominant {111} surface facet in such a morphology meets the requirement of the minimization of the mean surface energy. However, in the case of nanotube, elongating tubes along the $\langle 111 \rangle$ direction will lead to less {111} and more {110} facets on the surface and thereby higher mean surface energies of the nanocrystals, and the formation of nanotubes of other orientations such as [112] or [113]-oriented nanotube may be thermodynamically more favorable.[37] Our results not only demonstrate the ability to fabricate size-tunable magnetic hollow nanocrystals, but also show

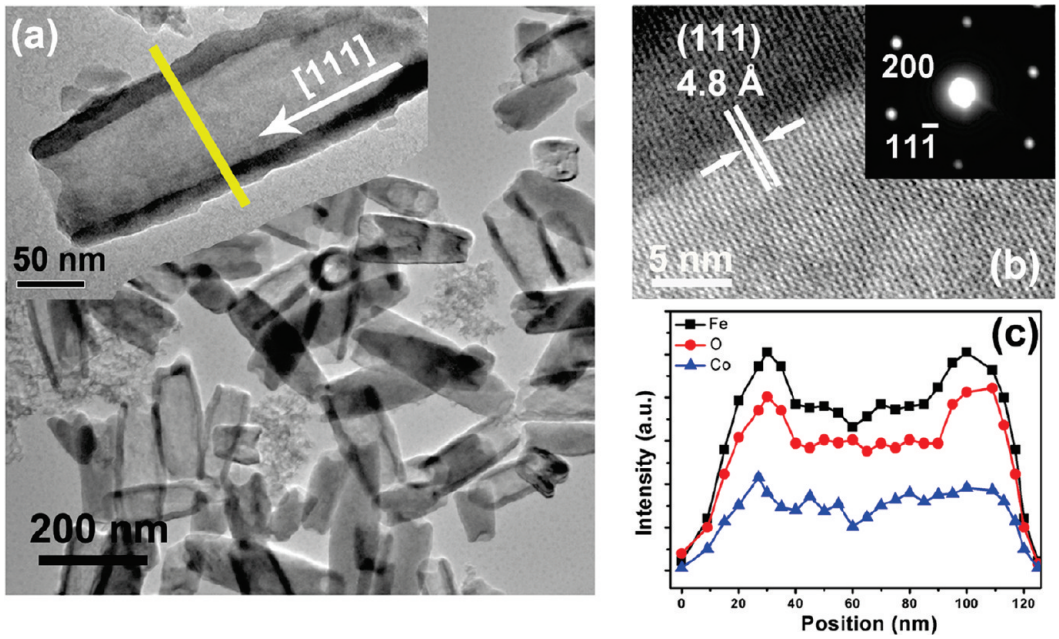

Figure 3. (a) TEM and (b) HRTEM of $CoFe_2O_4$ nanotubes. (c) EDS spectrum of a single $CoFe_2O_4$ nanotube. It reveals that the atomic ratio of Co:Fe:O across the tube (yellow line) is nearly constant and averaged to be 1:1.69: 4.92.

possible control of crystallographic orientation, and therefore the magnetic anisotropy, of the nanostructures.

MFe_2O_4 Nanotubes (M = Co, Mn, Ni, Cu). ***Characterizations of Microstructure and Composition.*** The MFe_2O_4 nanotubes were synthesized through introducing M^{2+} ion into single-crystalline α-Fe_2O_3 nanotube template. M hydroxides deposited on the surface α-Fe_2O_3 nanotube by wet chemical precipitation method were used as source for M^{2+} ions, and they are attached to Fe_2O_3 through the olation and oxolation bridges in alkaline condition.[39] The initial molar ratio of M^{2+} and Fe^{3+} in the reaction solution is about 0.65. Figure 3 shows the typical TEM images of the $CoFe_2O_4$ nanotubes. As can be seen in part a of Figure 3, tubular structure is also maintained in the $CoFe_2O_4$ products and no significant change in morphology with respect to α-Fe_2O_3 template is observed. The SAED and HRTEM results in Figure 3b indicate that the nanotubes are single-crystalline nature and elongated in [111] direction, which is similar to the case of Fe_3O_4 nanotubes. Energy-dispersive X-ray spectrum (EDS) confirms the existence of the elements Co, Fe, and O, with nearly uniform atomic ratios of 1:1.6:6.7 across the tube diameter as shown in Figure 3c. TEM images of other MFe_2O_4 (M = Ni, Mn, Cu) nanotubes are presented in Figure 4. Similar to the typical $CoFe_2O_4$ nanotube, they are (111)-oriented single-crystalline nanotubes. Most of the MFe_2O_4 nanocrystals have perfect hollow structure with solid wall. However, a few smaller irregular nanoparticles were also found in the TEM (Figure 4), which is either the metal oxides originated from the excess of $M(OH)_2$, or interrupted MFe_2O_4 nanotubes. The average molar ratio of M and Fe in the collective nanotubes is 0.56 $\pm$ 0.04 according to the EDS analysis (Figure S4 in the Supporting Information). XRD patterns of all MFe_2O_4 nanotubes are presented in Figure 5. All the diffraction peaks can be indexed as cubic spinel structure and no other impurities are observed, which agrees with TEM results.

Formation Mechanism. Unlike the core/shell solid−solid reaction in nanowire arrays system in which the shell was deposited by atomic layer deposition (ALD) or sputtering,[29,38] it has been found that the preanneal-

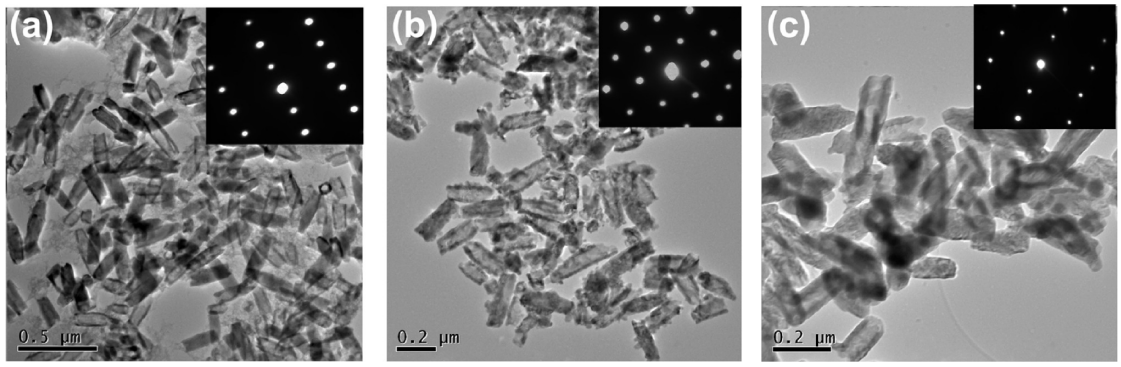

Figure 4. TEM images and SAED patterns of (a) $MnFe_2O_4$, (b) $NiFe_2O_4$, and (c) $CuFe_2O_4$, respectively.

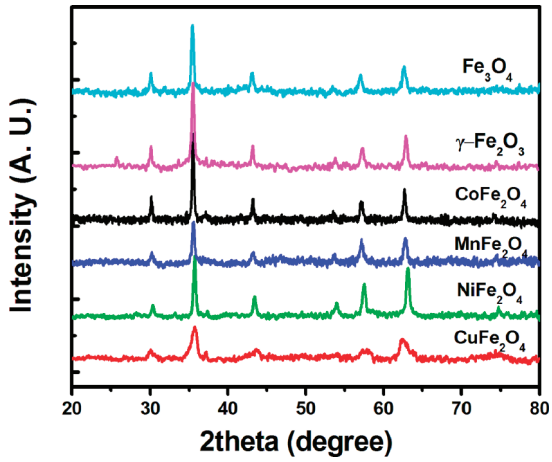

Figure 5. The XRD patterns of cubic spinel ferrites.

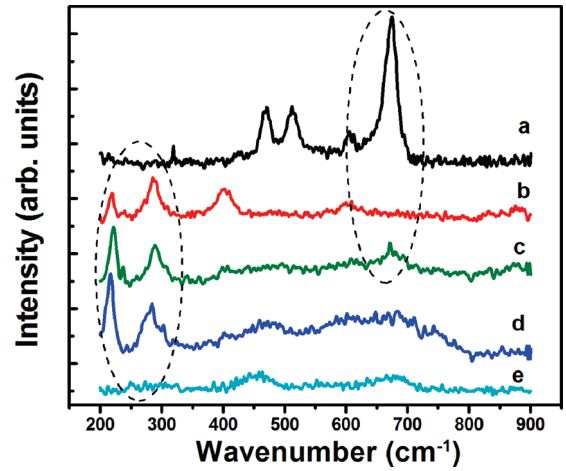

Figure 7. The Raman spectra of (a) as-prepared $Co(OH)_2$ powders, (b) α-Fe_2O_3 nanotubes, (c) α-Fe_2O_3/($Co(OH)_2$ + Co_3O_4) core/shell nanotubes, (d) $CoFe_2O_{4-x}$ nanotubes, (e) $CoFe_2O_4$ nanotubes.

ing of free-standing Fe_2O_3/$Co(OH)_2$ core/shell nanostructures in the presence of H_2 at a relative low temperature is a key step to produce MFe_2O_4 nanotubes. When Fe_2O_3/$Co(OH)_2$ core/shell nanotubes are directly annealed in air yields a mixture of nanorods and nanotubes as shown in part a of Figure 6. The XRD pattern in part b of Figure 6 indicates that the mixture consists of Co_3O_4 and Fe_2O_3. This is ascribed to the peeling off of Co hydroxide and oxides from the surface of Fe_2O_3 nanotubes induced by the local strain during the crystallization process of amorphous $Co(OH)_2$. It happens prior to the solid-state reaction and eventually leads to the formation of separate rodlike Co_3O_4 nanoparticles and Fe_2O_3 nanotubes. For a complete view of the formation process of MFe_2O_4 nanotubes, Raman analyses of the products in different reaction stage were carried out. Figure 7 shows the Raman spectra of the samples obtained from different reaction stages. Five Raman bands at 319, 468, 511, 610, and 678 cm^{-1} are found in the $Co(OH)_2$ sample prepared through chemical precipitation of Co^{2+} by NaOH using the same procedure as the coating process of Fe_2O_3/$Co(OH)_2$ (Figure 7a). The bands at 319 and 511 cm^{-1} are assigned to $E_u(T)$ and $A_{2u}(T)$ modes of $Co(OH)_2$.[40] The bands at 610 and 679 cm^{-1} are assigned to F_{2g} and A_{1g} mode of Co_3O_4.[41] The assignment of the band at 468 cm^{-1} is unclear. This band lies close to the frequencies of both $E_u(R)$ mode of $Co(OH)_2$ (433 cm^{-1}) and E_g mode of Co_3O_4 (482 cm^{-1}). Since the local strain induced by grain to grain contact of heterogeneous phases commonly causes a shift of Raman band, the assignment of $E_u(R)$ or E_g modes is presently uncertain. The Raman spectrum of as-prepared $Co(OH)_2$ reveals that the precipitation reaction at 60 °C produce a mixture of Co_3O_4 and $Co(OH)_2$. For the α-Fe_2O_3 nanotubes, the Raman band at 225 cm^{-1} is assigned to A_{1g} mode and the bands at 290 and 407 cm^{-1} are assigned to E_g modes[42] (Figure 7b). After precipitation of $Co(OH)_2$ on Fe_2O_3 nanotubes, three α-Fe_2O_3 characteristic Raman bands and A_{1g} band of Co_3O_4 are visible in Raman spectrum (Figure 7c). Despite that no obvious Raman band from $Co(OH)_2$ was observed in core/shell nanotubes, the shell should consist of both cobalt hydroxides and cobalt oxides by referring to the Raman analysis of as-prepared $Co(OH)_2$.

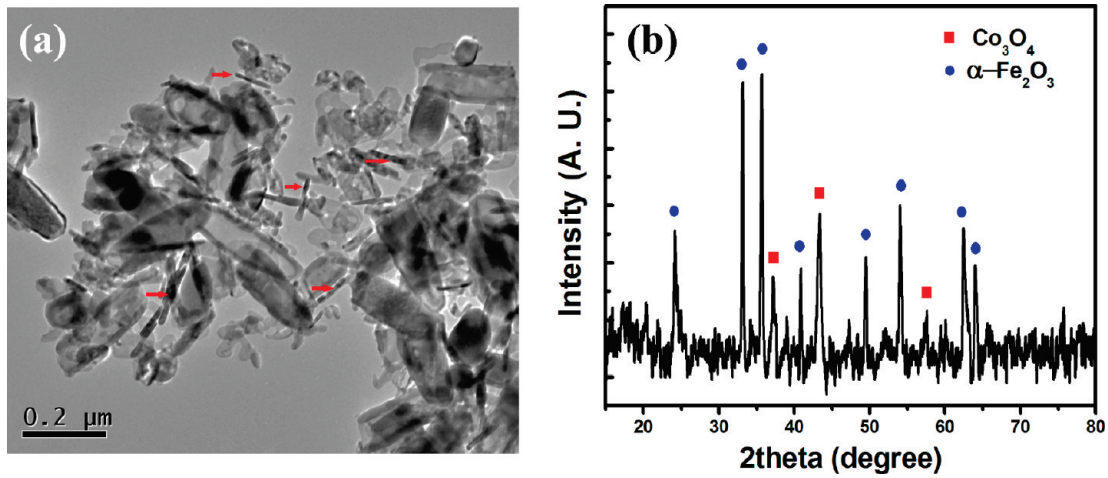

Figure 6. (a) TEM image and (b) XRD pattern of the sample obtained by direct annealing of α-Fe_2O_3/$Co(OH)_2$ core/shell nanotubes at 800 °C in air. Arrows indicate the rodlike nanoparticles.

The A_{1g} band disappears after preannealing under H_2 at 300 °C (Figure 7b). However, two Raman bands at 225 and 290 cm^{-1} from α-Fe_2O_3 are still observed, indicating that the product remains the α-Fe_2O_3 phase. TEM images of the Fe_2O_3/($Co(OH)_2$+Co_3O_4) before and after H_2 annealing are presented in Figure 8. From the TEM images, it can be seen that the $Co(OH)_2$ content fluctuates from one part to another along the nanotubes which is commonly observed in coating process.[38] Annealing in H_2 allows the $Co(OH)_2$ and Co_3O_4 to be reduced. At the same time, surface diffusion of Co cations along the nanotubes during the preannealing process improves composition homogeneity and results in MFe_2O_{4-x} ($0 < x < 1$) with a smooth surface. Finally, thermal annealing at high temperature (720 °C) in air activates the solid−solid reaction involving the interdiffusion of Co^{2+} and Fe^{3+} ions while the MFe_2O_{4-x} converts to cubic spinel $CoFe_2O_4$. This is consistent with the Raman spectrum of the sample after high temperature annealing, in which only two broad Raman bands at ~450 and 670 cm^{-1} which correspond to the modes of octahedral and tetrahedral sites in spinel ferrites are observed.[43] (Figure 7e) According to the Raman and TEM analyses of growth process of $CoFe_2O_4$, the formation mechanism of MFe_2O_4 nanotubes can be summarized in three stages: (1) formation of Fe_2O_3/$M(OH)_2$ core/shell nanotubes by chemical precipitation, (2) surface diffusion of M ions along the nanotube to form MFe_2O_{4-x} intermediate *via* low temperature annealing in H_2/Ar atmosphere and (3) interdiffusion of M^{2+} and Fe^{3+} ions in high temperature solid−solid reaction to form single-crystal spinel MFe_2O_4 nanotubes.

Transformation that retains structural and single crystalline features can occur in these nanotubes not only because they are more flexible and contain less defects, but also because they consist of single or finite domains, so that the reaction behavior is molecule-like, and they have large surface areas for gas−solid or solid−solid reaction. The strong correlation between the crystallographic orientations of the template and the products indicates that the transformation process should proceed by a quasi-coherent molecular isomerization, in which the bond distortion and ion motion reach a kinetic equilibrium. This hypothesis is supported by the experiment of reduction reaction in pure H_2 atmosphere in which faster reaction rate leads to the formation of multicrystalline Fe_3O_4 nanotubes. Considering the undesirable aggregation and sintering in thermal treatments, the solid−solid reaction can be expected to occur only in a certain temperature range. For the case of $CoFe_2O_4$, the solid−solid reaction is activated at a temperature higher than 650 °C. However, if the temperature is higher than 800 °C, the product would be in solid nanorods. This kind of phase transformation is ubiquitous in nanoscale materials, especially in transition metal nano-oxides. And it could be extended to fabricate many complex oxides nanotubes and nanorings by using various templates such as ZnO and MnO_2 nanotubes.

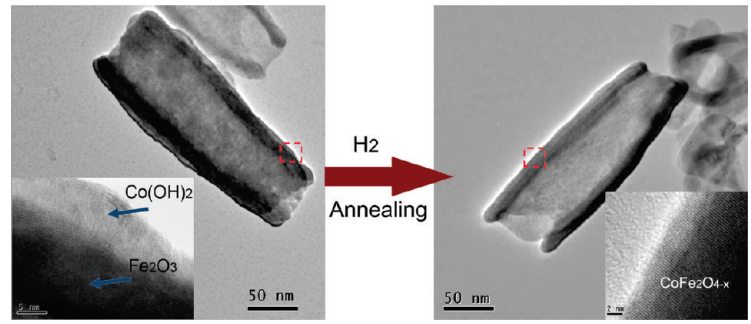

Figure 8. TEM images of α-Fe_2O_3/($Co(OH)_2$ + Co_3O_4) before and after H_2 preannealing.

Magnetic Properties of MFe_2O_4 Nanotubes. To understand the magnetic properties and their dependence on size, composition, and shape of the nanocrystals, the magnetic measurements of MFe_2O_4 nanotubes/nanorings were carried out by using a commercial SQUID magnetometer. For magnetite Fe_3O_4, all samples with different lengths showed soft magnetic behavior as shown in part a of Figure 9. Saturation magnetization (M_s) and coercivity (H_c) decrease with decreasing length (height) of the nanotubes (nanorings) due to finite size effect and shape anisotropy.[44] Compared with the magnetic nanoparticles of the same size, the high H_c in nanotubes (up to 320 Oe at 300 K) is ascribed to both "tube" structure and phosphate adsorbed on the surface of nanotubes, the latter is inherited from α-Fe_2O_3 template and would form spin pinning and block spin flip conversion.[45] As reported previously,[46,47] magnetic nanorings should have a stable vortex domain structure and possess an onion structure under a sufficiently high magnetic field. The sharpen change in H_c from the nanotube to nanoring may indicate the formation of vortex state in nanoring while it is absent in the nanotube due to their tubular morphology. The magnetic measurements of assembled magnetite nanoring array in part c of Figure 9 at 5 K confirmed the vortex and onion structures. As shown in part d of Figure 9, the magnetite nanorings array shows much smaller out-of-plane magnetization, analogous to the observation in Co nanorings arrays.[48] While the in-plane hysteresis loop shows two distinct switching fields: one at about 0.28 kOe and the other at a much higher value of 10 kOe, which corresponds to the transition from the onion state to vortex state.[46−48] For other spinel ferrite samples, the magnetic measurement was focused on nanotubes with a length of 220−260 nm to show their dependence on composition. The hysteresis loops of MFe_2O_4 at 300 K in part b of Figure 9 show the composition-dependent M_s and H_c. It can be seen that the $CoFe_2O_4$ ferrite nanotubes exhibit a high coercivity of 1.0 kOe at room temperature as Co ferrite possesses higher magnetocrystal-

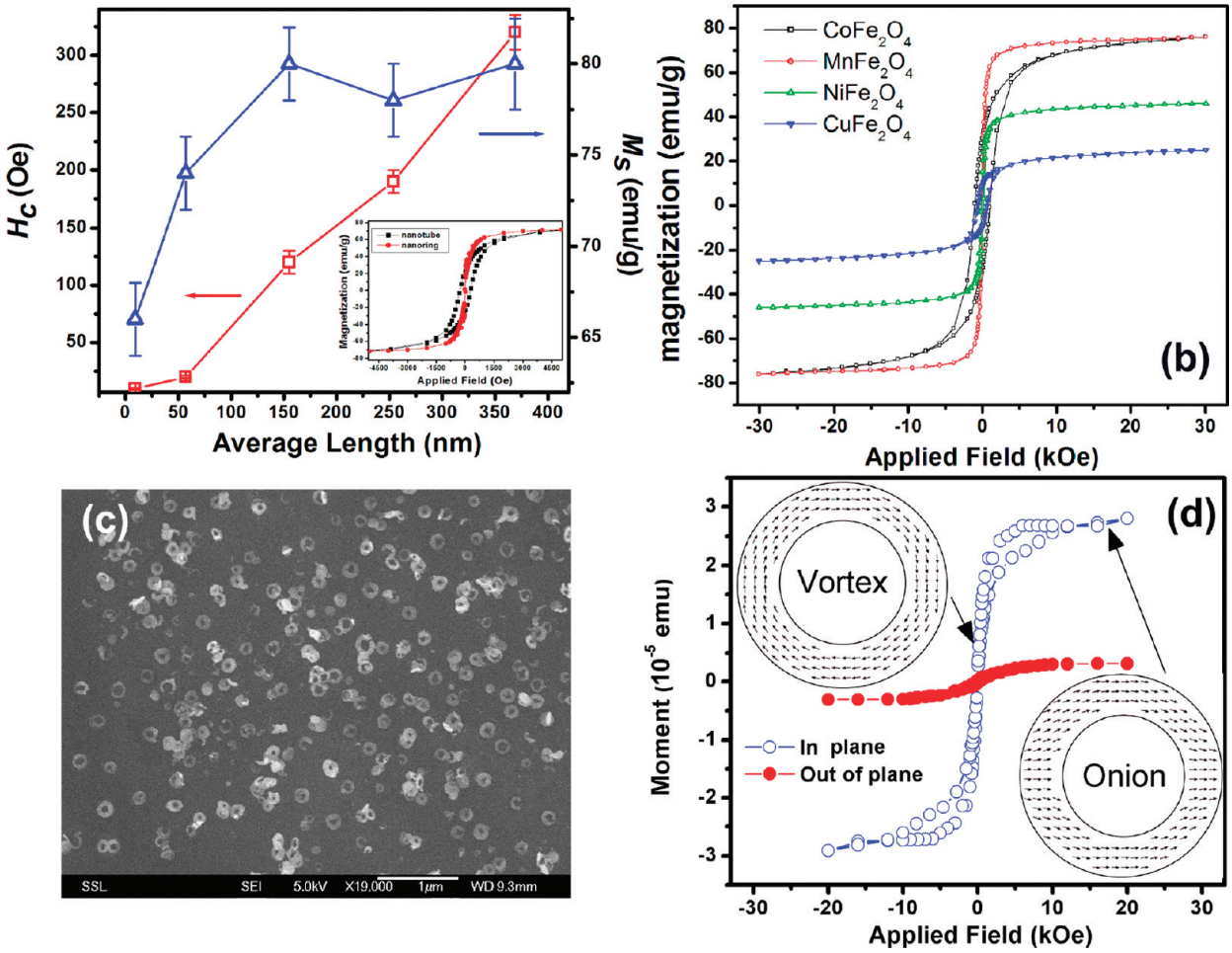

Figure 9. (a) The coercivity (H_c) and saturation magnetization (M_s) dependences on length of magnetite nanotubes/nanorings at 300 K. The inset is the typical hysteresis loops of magnetite nanotubes (length = 370 nm) and nanorings (thickness = 50 nm). (b) The hysteresis loops of MFe_2O_4 (M = Co, Mn, Ni, Cu) nanotubes at 300 K. (c) SEM image of assembled magnetite nanorings array. (d) The in-plane and out-of-plane hysteresis loop of assembled magnetites nanorings array with thickness of 10 nm at 5 K. The insets are the schematic illustrations of onion and vortex state in nanoring structure.

TABLE 1. Comparison of the Catalytic Kinetic Parameters of Fe_3O_4 Nanotubes and Nanoparticles[a]

samples	[E] (M)	substrate	K_m (mM)	V_{max} (M s^{-1})	K_{cat}(s^{-1})
Fe_3O_4 nanotubes (370 nm in length)	5.30×10^{-10}	TMB	4.147	5.2×10^{-6}	9.81×10^5
Fe_3O_4 nanoparticles (300 nm in diameter)	11.4×10^{-13}	TMB	0.098	3.44×10^{-8}	3.02×10^4

[a] [E] is the concentration of nanotubes or nanoparticles, K_m is the Michaelis constant, V_{max} is the maximal reaction velocity, and K_{cat} is the catalytic constant, where $K_{cat} = V_{max}/[E]$. The parameters of Fe_3O_4 nanoparticles are obtained from ref 14.

line anisotropy. Soft magnetic properties were observed in $MnFe_2O_4$ and $NiFe_2O_4$, while a relatively high coercivity was found for $CuFe_2O_4$. The magnetic characterizations show that these spinel nanotubes/nanorings have the capability of tuning magnetic properties by size, shape, and composition for diverse bioapplications such as magnetic resonance image (MRI), hyperthermia, cell label, drug delivery, and so forth.

Biological Applications. ***Peroxidase-like Activity of Fe_3O_4 Nanotubes.*** Given the hollow structure with large surface areas, these biocompatible nanotubes/nanorings are expected to have advantages in catalytic applications. For example, recently an intrinsic peroxidase-like catalytic property has been discovered in Fe_3O_4 nanoparticles, which is widely used for laboratory immunoassays.[15] Here we carried out similar measurements on Fe_3O_4 nanotubes to examine its catalytic property (Figure S5 in the Supporting Information). The direct comparison of the results obtained from magnetite nanotubes and nanoparticles are summarized in Table 1. The catalytic constant (K_{cat}) of the magnetite nanotubes (370 nm in length) is larger than that of spherical nanocrystals (300 nm in diameter) by an order of magnitude, which is due to the relative larger surface area (measured BET surface of ~38 m^2/g). The result suggests that these Fe_3O_4 nanotubes/nanorings could be a high efficient enzyme mimic agent in the application of immunoassay test.

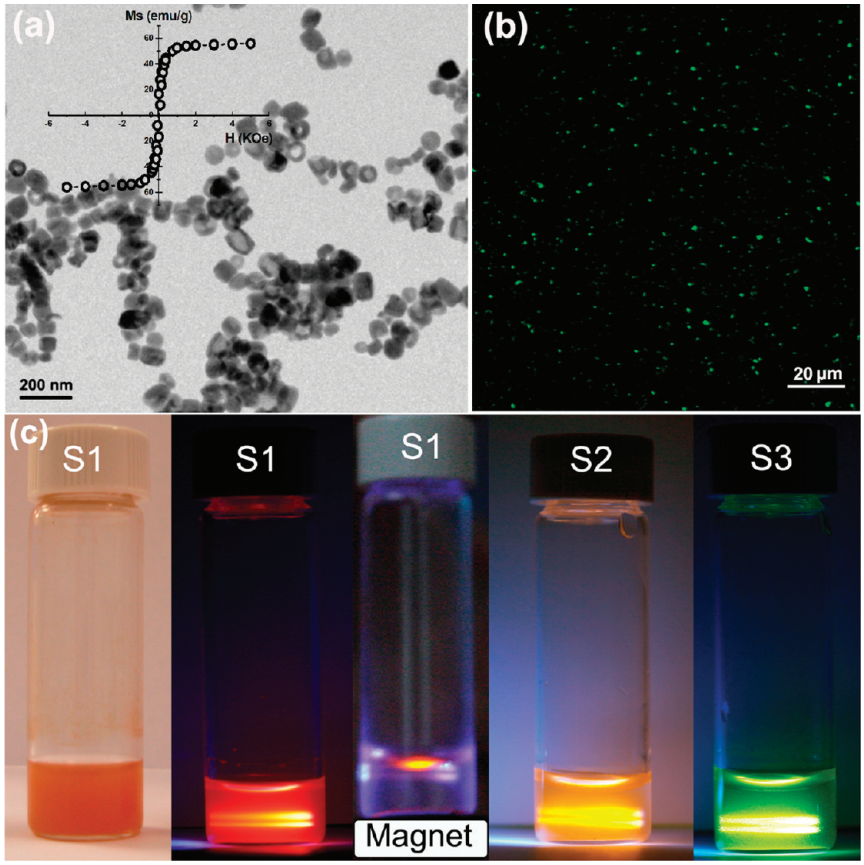

Figure 10. (a) TEM images of nanocomposites. The insert is the hysteresis loop of nanocomposites at 300 K; (b) luminescence images of nanocompostes; (c) optical images of the different nanocomposites in aqueous solution without/with UV laser irradiation.

Luminescent Magnetic Nanocomposites for Magnetic Separation and Optical Probe of Cancer Cell. To further demonstrate the utility of these magnetic nanotubes/nanorings in biological applications, the uniform γ-Fe_2O_3 nanorings with height of 50 nm were used as the nanocapsule to fabricate luminescent/magnetic nanocomposite particles for magnetic separation and optical detection of lung cancer cells. The γ-Fe_2O_3 nanorings are chosen here because they have good transparent properties for fluorescence probe of labeled cells, vortex domain structure for weak interparticle magnetic interaction, high saturation magnetization under a small external field for magnetic separation. Highly luminescent CdSe/ZnS QDs of red, yellow, and green emission colors purchased from Evident Technologies were loaded into polymer maghemite nanorings by an ultrasonication treatment. The carried QDs endowed the optical characteristics to maghemite nanorings for optical detection of labeled cell. Figure 10a shows a representative TEM of luminescent/magnetic nanocomposites. Ring-like structure of the nanocomposites is readily observed. The saturation magnetization of the nanocomposites is about 60 emu/g at room temperature as shown in the inset of Figure 10a. A fluorescence scanning microscopy image of nanocomposites particle is presented in part b of Figure 10, a better signal-to-background ratio of over 30 is observed in these digital image. The optical images in part c of Figure 10 show that the obtained nanocomposites are water-soluble with minimal or no aggregation. Under the laser excitation, strong light emission is observed. The FWHMs of the emission bands (~40 nm) for these nanocomposites are comparable to that of pure QDs in chloroform, however, the fluorescent lifetime is reduced from 32 $\pm$ 2 to 16 $\pm$ 2 ns due to the solvent change and possible changes on the surface of the QDs during the encapsulation process.(Figure S6 in Supporting Information) As the vortex domain structure in nanocomposites possess much higher saturation magnetization and can be easily saturated with a relatively small field, the labeled cells can be separated efficiently by applying a external field (~1000 Oe) using a permanent magnet. On the contrary, a typical superparamagnetic nanocrystals show much lower magnetization (<10 emu/g) under same external field. The optical and fluorescent images of the separated lung cancer cell are shown in parts a and b of Figure 11. The cell separation experiment described here demonstrates the advantages of this kind of vortex nanorings

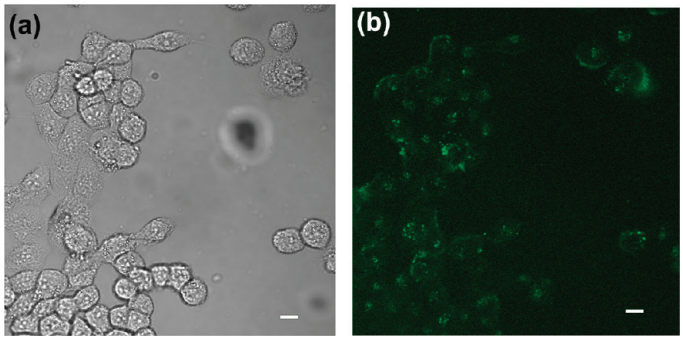

Figure 11. (a) Optical and (b) luminescence images of the lung cancer cell labeled with the luminescent/magnetic nanocomposite. Scale bar is 10 μm.

dispersion, namely, a much higher magnetic susceptibility can be obtained at lower magnetic fields through a vortex to onion transition. This behavior is also important for other biomedical and biomagnetic applications such as drug delivery, MRI, and hyperthermia.

CONCLUSION

In summary, we have developed a new universal template route for the fabrication of MFe_2O_4 nanotubes/nanorings *via* a simple thermal transformation process. The magnetic cubic spinel MFe_2O_4 synthesized in this manner maintains the tubular morphology and single crystal features. The crystallographic orientation of nanotubes/nanorings shows strong correlation with their morphologies during the thermal transformation process. These cubic spinel nanotubes and nanorings exhibit unique size-, shape-, and composition-dependent magnetic properties. They have been shown the advantages in applications as a high effective peroxidase mimic catalyst or as a general nanocapsule hybridized with luminescent QDs for magnetic separation and optical probe of lung cancer cells. The successful synthesis of these magnetic MFe_2O_4 nanotubes/nanorings opens up opportunities for improving existing biological applications and designing novel technologies in the future.

METHODS

Synthesis of α-Fe_2O_3 NTs and NRs. α-Fe_2O_3 nanotubes/nanorings with various lengths or thicknesses were synthesized by a hydrothermal treatment of $FeCl_3$ solution in the presence of $NH_4H_2PO_4$ at 220 °C. By adjusting the concentration of reactants, various sized α-Fe_2O_3 nanostructures were produced. Detailed process has been reported in literature.[21,30,32]

Synthesis of Fe_3O_4 and γ-Fe_2O_3 NTs and NRs. Fe_3O_4 and γ-Fe_2O_3 NTs and NRs were prepared by direct solid−gas reaction. In brief, 0.5 g of α-Fe_2O_3 nanotubes was heated in a horizontal quartz tube furnace at 420 °C for 120 min under a constant flow of 5% H_2/95% Ar at 800 sccm. Then the furnace was cooled down to room temperature without any changes in atmosphere. The black Fe_3O_4 product was collected from the small quartz. Annealing of as-prepared Fe_3O_4 nanotubes (nanorings) in an open tube furnace at 280 °C for 120 min yields γ-Fe_2O_3 nanotubes (nanorings). The assembly of thin magnetite nanorings was prepared on Si substrate by the following procedure: a few drops of α-Fe_2O_3 nanorings aqueous dispersion (0.02 mg/mL) was dropped into chloroform solution in a glass beaker with diameter ~5 cm to form a thin water membrane. A surface-modified hydrophilic Si (100) substrate was vertically immersed into chloroform solution and then slowly pulled up. The α-Fe_2O_3 nanoring arrays formed on the Si substrate were then transformed into arrays of magnetite nanorings by thermal reduction reaction.

Synthesis of MFe_2O_4 Nanotubes. MFe_2O_4 nanotubes were prepared by solid−solid reaction of α-Fe_2O_3 nanotubes with coated metal hydroxide shell. Here we take $CoFe_2O_4$ nanotubes as an example. In a typical procedure, 2.5 mL of 0.1 M $CoSO_4$ solution was added into 20 mL of 0.01 M α-Fe_2O_3 aqueous suspension. The mixture was heated to 60 °C with magnetic stirring, and then 40 mL of 0.01 M NaOH was added into the solution under vigorous stirring. The stirring was kept for 30 min at 60 °C. After the reaction was completed, the Fe_2O_3/$Co(OH)_2$ core/shell precipitation was separated by centrifugation and dried at 60 °C. The resultant Fe_2O_3/$Co(OH)_2$ core/shell sample was first annealed for 30 min under a constant flow of 5% H_2/95% Ar at 800 sccm at 300 °C, and then annealed in air at 720 °C for 3 h to activate the interfacial solid−solid reaction. $MnFe_2O_4$, $NiFe_2O_4$, and $CuFe_2O_4$ were prepared similarly, using manganese acetate, nickel chloride, and copper sulfate, respectively, as reactant. All the reagents were of analytical purity purchased from Sigma-Aldrich Co.

Synthesis of Luminescent and Magnetic Nanocomposites. To achieve dual functional nanocomposites, polymer γ-Fe_2O_3 nanorings were first prepared by deposition of positively charged poly(ethyleneimine) (PEI, 50% w/v) with NH_2 (NH^{3+}) group on the surface of γ-Fe_2O_3 nanorings. Typically, 2 mL of PEI (2 mg/mL) was added into 30 mL of 2 mg/mL γ-Fe_2O_3 nanorings aqueous dispersion (pH was preadjusted to ~3 by 1.0 mol/mL of HCl), followed by a ultrasonication to prepare colloidal polymer γ-Fe_2O_3 nanorings. It was then washed several times with deionized water by magnetic decantation. To carry out the coupling reaction, 0.5 mL of CdSe/ZnS QDs (80 nmol/mL) and 0.5 mL of polymer γ-Fe_2O_3 nanorings (5 mg/mL) were transferred into a 20 mL mixture of chloroform/ethanol/water (2:5:5) under sonication. The suspension was treated in ultrasonic bath for 40 min to form the nanocomposite. The luminescent and magnetic nanocomposites were magnetically separated from the solution and washed several times with deionized water.

Steady-State Kinetic Assays of Peroxidase-like Activity of Fe_3O_4 Nanotubes. A 20 μg portion of Fe_3O_4 nanotubes with an average length of 370 nm were ultrasonically dispersed into 500 μL buffer solution (0.2 M NaAc, pH 3.5) in the presence of 530 mM H_2O_2; 816 mM 3,3,5,5-tetramethylbenzidine (TMB) was used as the substrates. The steady-state kinetic assays were carried out at 30 °C. All the reactions were monitored in time scan mode at 650 nm using a Shimadzu UV-1700 spectrophotometer.

Magnetic Separation and Optical Probe of Cancer Cell. A431 cell lines originated from human carcinoma of the lung were obtained from the American type Culture Collection, USA. A 3.0 mg portion of EDC ((1-ethyl-3-[3-dimethylaminopropyl]-carbodiimide hydrochloride) were first added into 1 mL of 0.1 mg/mL nanocomposite phosphate-buffered saline (PBS) solution and mixed thoroughly using a vortex mixer, then 2 μg/mL of the antibody was added and kept at 4 °C for the reaction overnight. The antibody-functionalized QD was washed with PBS, and stored at 4 °C until needed. A few drops of the functionalized nanocomposite were added to a 1 mL A431 lung cancer cell suspension containing 10 000 cells/mL. Following 5 min of incubation at room temperature under gentle shaking, the cells were separated from the suspension using a permanent magnet. The labeled cells were observed using a laser scanning confocal fluorescence microscopy.

Characterization. The structure of the materials were examined by a Bruker D/MAX 2500 X-ray diffractometer with Cu Kα radiation $\lambda = 1.54056$ Å). TEM and HRTEM analysis, selected-area electron diffraction (SAED), and energy-dispersive X-ray spectroscopy (EDS) were performed with a field-emission transmission electron microscope (TEM, JEOL, JEM 2010, accelerating voltage 200 KV). Raman spectroscopy study was carried out by a micro-Raman system (Jobin-Yvon T64000) with a typical laser power of ~0.2 mW. Magnetic properties were measured using a MPMSXL-5 Quantum Design superconducting quantum interference device magnetometer (SQUID) with a field up to 5 T. Confocal fluorescence imaging was performed using Carl Zeiss LSM 510 with a 488 nm excitation line using a 20 × /0.25 microscope objective.

Acknowledgment. The authors would like to thank Prof. Ping Chen and Dr. Zhi Tao Xiong for TPR measurements and Prof. Chrong Haur Sow and Dr. Zhi Kui Wang for discussion. This work was supported by the Ministry of Education (MOE) Academic Research Fund under Grants R-144-000-209-112.

Supporting Information Available: TPR profiles of α-Fe2O3 nanotubes and nanorings. Size distribution histograms of Fe_3O_4 nanotubes and nanorings. TEM and HRTEM images of Fe_3O_4 nanotubes and nanorings of different crystallographic orientations. EDS of MFe_2O_4 nanotubes. The steady-state kinetic assay of peroxidase-like activity of Fe_3O_4 nanotubes. The photoluminescence and fluorescent lifetime of nanocompoistion. This material is available free of charge *via* the Internet at http://pubs.acs.org.

REFERENCES AND NOTES

1. Seo, W. S.; Lee, J. H.; Sun, X. M.; Suzuki, Y.; Mann, D.; Liu, Z.; Terashima, M.; Yang, P. C.; Mcconnell, M. V.; Nishimura, D. G.; Dai, H. J. FeCo/Graphitic-Shell Nanocrystals as Advanced Magnetic-Resonance-Imaging and Near-Infrared Agents. *Nat. Mater.* **2006**, *5*, 971–976.
2. Park, J.; An, K.; Hwang, Y.; Park, J. G.; NOH, H. J.; Kim, J. Y.; Park, J. H.; Hwang, N. M.; Hyeon, T. Ultra-Large-Scale Syntheses of Monodisperse Nanocrystals. *Nat. Mater.* **2004**, *3*, 891–895.
3. O'Handley, R. C. *Modern Magnetic Materials—Principles and Applications*; John Wiley & Sons: New York, 2000.
4. Sun, S. H.; Zeng, H.; Robinson, D. B.; Raoux, S.; Rice, P. M.; Wang, S. X.; Li, G. X. Monodisperse MFe_2O_4 (M = Fe, Co, Mn) Nanoparticles. *J. Am. Chem. Soc.* **2003**, *126*, 273–279.
5. Deng, H.; Li, X. L.; Peng, Q.; Wang, X.; Chen, J. P.; Li, Y. D. Monodisperse Magnetic Single-Crystal Ferrite Microspheres. *Angew. Chem., Int. Ed.* **2005**, *44*, 2782–2785.
6. Cornell, R. M. Schwertmann, U. *The Iron Oxides: Structure, Properties, Reactions, Occurrence and Uses;* Wiley-VCH: New York, 2003; pp 126−136.
7. Redl, F. X.; Black, C. T.; Papaefthymiou, G. C.; Sandstrom, R. L.; Yin, M.; Zeng, H.; Murray, C. B.; O'Brien, S. P. Magnetic, Electronic, and Structural Characterization of Nonstoichiometric Iron Oxides at the Nanoscale. *J. Am. Chem. Soc.* **2004**, *126*, 14583–14599.
8. Chang, M. T.; Chou, L. J.; Hsien, C. H.; Chueh, Y. L.; Wang, Z. L.; Murakami, Y.; Shindo, D. Magnetic and Electrical Characterizations of Half-Metallic Fe_3O_4 Nanowires. *Adv. Mater.* **2007**, *19*, 2290–2295.
9. Weiss, W.; Zscherpel, D.; Schlogl, R. On the Nature of the Active Site for the Ethylbenzene Dehydrogenation over Iron Oxide Catalysts. *Catal. Lett.* **1998**, *52*, 215–220.
10. Bergemann, C.; Muller-Schulte, D.; Oster, J.; Brassard, L.; Lubbe, A. S. Magnetic Ion-Exchange Nano- and Microparticles for Medical, Biochemical and Molecular Biological Applications. *J. Magn. Magn. Mater.* **1999**, *194*, 45–52.
11. Lee, H.; Yu, M. K.; Park, S.; Moon, S.; Min, J. J.; Jeong, Y. Y.; Kang, H. W.; Jon, S. Thermally Cross-Linked Superparamagnetic Iron Oxide Nanoparticles: Synthesis and Application as a Dual Imaging Probe for Cancer *in Vivo*. *J. Am. Chem. Soc.* **2007**, *129*, 12739–12745.
12. Dobson, J. Gene Therapy Progress and Prospects: Magnetic Nanoparticle-Based Gene Delivery. *Gene Ther.* **2006**, *13*, 283–287.
13. Perez, J. M.; Josephson, L.; O' Loughlin, T.; Hogemann, D.; Weissleder, R. Magnetic Relaxation Switches Capable of Sensing Molecular Interactions. *Nat. Biotechnol.* **2002**, *20*, 816–820.
14. Louie, A. Y.; Huber, M. M.; Ahrens, E. T.; Rothbacher, U.; Moats, R.; Jacobs, R. E.; Fraser, S. E.; Meade, T. J. *In Vivo* Visualization of Gene Expression using Magnetic Resonance Imaging. *Nat. Biotechnol.* **2000**, *18*, 321–325.
15. Gao, L. Z.; Zhuang, J.; Nie, L.; Zhang, J. B.; Zhang, Y.; Gu, N.; Wang, T. H.; Feng, J.; Yang, D. L.; Perrett, S.; Yan, X. Y. Intrinsic Peroxidase-like Activity of Ferromagnetic Nanoparticles. *Nat. Nanotechnol.* **2007**, *2*, 577–583.
16. Bae, S.; Lee, S. W.; Takemura, Y. Applications of $NiFe_2O_4$ Nanoparticles for a Hyperthermia Agent in Biomedicine. *Appl. Phys. Lett.* **2006**, *89*, 252503(1−3).
17. Ziolo, R. F.; Giannells, E. P.; Weinstein, B. A.; Ohoro, M. P.; Ganguly, B. N.; Mehrotra, A. V.; Russell, M. W.; Huffman, D. R. Matrix-Mediated Synthesis of Nanocrystalline γ-Fe_2O_3—A New Optically Transparent Magnetic Material. *Science* **1992**, *257*, 219–223.
18. Wang, D.; He, J.; Rosenzweig, N.; Rosenzweig, Z. Rational Growth of Branched and Hyperbranched Nanowire Structures. *Nano Lett.* **2004**, *4*, 409–413.
19. Woo, K.; Hong, J.; Choi, S.; Lee, H.; Ahn, J.; Kim, C. S.; Lee, S. W. Easy Synthesis and Magnetic Properties of Iron Oxide Nanoparticles. *Chem. Mater.* **2004**, *16*, 2814–2818.
20. Remskar, M. Inorganic Nanotubes. *Adv. Mater.* **2004**, *16*, 1497–1504.
21. Jia, C. J.; Sun, D. S.; Luo, F.; Han, X. D.; Heyderman, L. J.; Yan, Z. G.; Yan, C. H.; Zheng, K.; Zhang, Z.; Takano, M.; *et al.* Large-Scale Synthesis of Single-Crystalline Iron Oxide Magnetic Nanorings. *J. Am. Chem. Soc.* **2008**, *130*, 16968–16977.
22. Piao, Y.; Kim, J.; Bin, Na H.; Kim, D.; Baek, J. S.; Ko, M. K.; Lee, J. H.; Shokouhimehr, M.; Hyeon, T. Wrap−Bake−Peel Process for Nanostructural Transformation from β-FeOOH Nanorods to Biocompatible Iron Oxide Nanocapsules. *Nat. Mater.* **2008**, *7*, 242–247.
23. Murray, C. B.; Kagan, C. R.; Bawendi, M. G. Synthesis and Characterization of Monodisperse Nanocrystals and Close-Packed Nanocrystal Assemblies. *Annu. Rev. Mater. Sci.* **2000**, *30*, 545–610.
24. Schmidt, O. G.; Eberl, K. Nanotechnology—Thin Solid Films Roll Up into Nanotubes. *Nature* **2001**, *410*, 168.
25. Li, Y. D.; Li, X. L.; He, R.; Zhu, J.; Deng, Z. X. Artificial Lamellar Mesostructures to WS_2 Nanotubes. *J. Am. Chem. Soc.* **2002**, *124*, 1411–1416.
26. Goldberger, J.; He, R. R.; Zhang, Y. F.; Lee, S. W.; Yan, H. Q.; Choi, H. J.; Yang, P. D. Single-Crystal Gallium Nitride Nanotubes. *Nature* **2003**, *422*, 599–602.
27. Liu, Z. Q.; Zhang, D. H.; Han, S.; Li, C.; Lei, B.; Lu, W. G.; Fang, J. Y.; Zhou, C. W. Single Crystalline Magnetite Nanotubes. *J. Am. Chem. Soc.* **2005**, *127*, 6–7.
28. Jiao, F.; Jumas, J. C.; Womens, M.; Chadwick, A. V.; Harrison, A.; Bruce, P. G. Synthesis of Ordered Mesoporous Fe_3O_4 and γ-Fe_2O_3 with Crystalline Walls Using Post-Template Reduction/Oxidation. *J. Am. Chem. Soc.* **2006**, *128*, 12905–12909.
29. Fan, H. J.; Knez, M.; Scholz, R.; Nielsch, K.; Pippel, E.; Hesse, D.; Zacharias, M.; Gösele, U. Monocrystalline Spinel Nanotube Fabrication Based on the Kirkendall Effect. *Nat. Mater.* **2006**, *5*, 627–631.
30. Jia, C. J.; Sun, L. D.; Yan, Z. G.; You, L. P.; Luo, F.; Han, X. D.; Pang, Y. C.; Zhang, Z.; Yan, C. H. Single-Crystalline Iron Oxide Nanotubes. *Angew. Chem., Int. Ed.* **2005**, *44*, 4328–4333.
31. Hu, X. L.; Yu, J. C.; Gong, J. M.; Li, Q.; Li, G. S. α-Fe_2O_3 Nanorings Prepared by a Microwave-Assisted Hydrothermal Process and Their Sensing Properties. *Adv. Mater.* **2007**, *19*, 2324–2329.
32. Fan, H. M.; You, G. J.; Li, Y.; Zheng, Z.; Tan, H. R.; Shen, Z. X.; Tang, S. H.; Feng, Y. P. Shape Controlled Synthesis of Single-Crystalline Fe_2O_3 Hollow Nanocrystals and Their Tunable Optical Properties. *J. Phys. Chem. C* **2009**, *113*, 9928–9935.
33. Kostorz, G. *Phase Transformations in Materials*; Wiley-VCH: Weinheim, Germany, 2001.
34. Son, D. H.; Hughes, S. M.; Yin, Y. D.; Alivisatos, A. P. Cation Exchange Reactions in Ionic Nanocrystals. *Science* **2004**, *306*, 1009–1012.
35. Becker, P. P.; Heizmann, J. J.; Baro, R. Relations Topotaxiques entre des Cristaux Naturels D'Hématite et la Magnétite qui en est Issue par Réduetion à Basse Température. *J. Appl. Crystallogr.* **1977**, *10*, 77–78.
36. Bursill, L. A.; Withers, R. L. On the Multiple Orientation Relationships between Hematite and Magnetite. *J. Appl. Crystallogr.* **1979**, *12*, 287–294.
37. Wang, Z. W.; Daemen, L. L.; Zhao, Y. S.; Zha, C. S.; Downs, R. T.; Wang, X. D.; Wang, Z. L.; Hemley, R. J. Morphology-Tuned Wurtzite-type ZnS Nanobelts. *Nat. Mater.* **2005**, *4*, 922–927.
38. Yang, Y.; Sun, X. W.; Tay, B. K.; Wang, J. X.; Dong, Z. L.; Fan,

H. M. Twinned Zn_2TiO_4 Spinel Nanowires Using ZnO Nanowires as a Template. *Adv. Mater.* **2009**, *19*, 1839–1845.
39. Govender, K.; Boyle, D. S.; Kenway, P. B.; O'Brien, P. Understanding the Factors that Govern the Deposition and Morphology of Thin Films of ZnO from Aqueous Solution. *J. Mater. Chem.* **2004**, *14*, 2575–2591.
40. Shieh, S. R.; Duffy, T. S. Raman Spectroscopy of $Co(OH)_2$ at High Pressures: Implications for Amorphization and Hydrogen Repulsion. *Phys. Rev. B* **2002**, *66*, 134301.
41. Hadjievl, V. G.; Ilievl, M. N.; Vergilov, I. V. The Raman Spectra of Co_3O_4. *J. Phys. C: Solid State Phys.* **1988**, *21*, L199–L211.
42. deFaria, D. L. A.; Silva, S. A.; deOliveira, M. T. Raman Microspectroscopy of Some Iron Oxides and Oxyhydroxides. *J. Raman. Spectrosc.* **1997**, *28*, 873–878.
43. Yu, T.; Shen, Z. X.; Shi, Y.; Ding, J. Cation Migration and Magnetic-Ordering in Spinel $CoFe_2O_4$ Powder: Micro-Raman Scattering Study. *J. Phys.: Condens. Mater.* **2002**, *14*, L613−L618.
44. Adeyeye, A. O.; Bland, J. A. C.; Daboo, C.; Hasko, D. G. Magnetostatic Interactions and Magnetization Reversal in Ferromagnetic Wires. *Phys. Rev. B* **1997**, *56*, 3265–3270.
45. Lv, B. L.; Xu, Y.; Wu, D.; Sun, Y. H. Preparation and Properties of Magnetic Iron Oxide Nanotubes. *Particuology* **2008**, *6*, 344–339.
46. Rothman, J.; Klaui, M.; Lopez-Diaz, L.; Vaz, C. A. F.; Bleloch, A.; Bland, J. A. C.; Cui, Z.; Speaks, R. Observation of a Bi-Domain State and Nucleation Free Switching in Mesoscopic Ring Magnets. *Phys. Rev. Lett.* **2001**, *86*, 1098–1101.
47. Zhu, F. Q.; Chern, G. W.; Tchernyshyov, O.; Zhu, X. C.; Zhu, J. G.; Chien, C. L. Magnetic Bistability and Controllable Reversal of Asymmetric Ferromagnetic Nanorings. *Phys. Rev. Lett.* **2006**, *96*, 027205.
48. Zhu, F. Q.; Fan, D. L.; Zhu, X. C.; Zhu, J. G.; Cammarata, R. C.; Chien, C. L. Ultrahigh-Density Arrays of Ferromagnetic Nanorings on Macroscopic Areas. *Adv. Mater.* **2004**, *16*, 2115–2159.